Structural Engineering and Mechanics, *Vol. 68, No. 3 (2018) 299-312*
DOI: https://doi.org/10.12989/sem.2018.68.3.299

An extended finite element method for modeling elastoplastic FGM plate-shell type structures

Hanen Jrad*[2], Jamel Mars[2a], Mondher Wali[1,2b] and Fakhreddine Dammak[2c]

[1]*Department of Mechanical Engineering, College of Engineering, King Khalid University, Abha, Saudi Arabia*
[2]*Engineering Production Mechanics and Materials Unit (UGPMM), National Engineering School of Sfax, University of Sfax, B.P. 1173-3038, Sfax, Tunisia*

(Received May 25, 2018, Revised August 6, 2018, Accepted August 8, 2018)

Abstract. In this paper, an extended finite element method is proposed to analyze both geometric and material non-linear behavior of general Functionally Graded Material (FGM) plate-shell type structures. A user defined subroutine (UMAT) is developed and implemented in Abaqus/Standard to study the elastoplastic behavior of the ceramic particle-reinforced metal-matrix FGM plates-shells. The standard quadrilateral 4-nodes shell element with three rotational and three translational degrees of freedom per node, S4, is extended in the present study, to deal with elasto-plastic analysis of geometrically non-linear FGM plate-shell structures. The elastoplastic material properties are assumed to vary smoothly through the thickness of the plate-shell type structures. The nonlinear approach is based on Mori-Tanaka model to underline micromechanics and locally determine the effective FGM properties and self-consistent method of Suquet for the homogenization of the stress-field. The elasto-plastic behavior of the ceramic/metal FGM is assumed to follow Ludwik hardening law. An incremental formulation of the elasto-plastic constitutive relation is developed to predict the tangent operator. In order to to highlight the effectiveness and the accuracy of the present finite element procedure, numerical examples of geometrically non-linear elastoplastic functionally graded plates and shells are presented. The effects of the geometrical parameters and the volume fraction index on nonlinear responses are performed.

Keywords: composites; finite element method (FEM); functionally graded; non-linear analysis; numerical methods; plate/shell structures

1. Introduction

Composite materials play significant role in advanced mechanical and structural applications. They have found increasing use with the rapid development of industries because they offer advantages over conventional materials. As one of the important structural components, composite laminated plates and shells, which are widely used in various engineering applications, such as airplanes, naval vehicles aircrafts, pressure vessels and civil industries. However, laminated plates and shells can present large stress discontinuities due to great mismatch in material properties, which induce a premature delamination, warping and cracking. Recently, functionally graded materials (FGM) has found extensive applications as structural elements in contemporary industries such as aeronautics production industry, mechanical engineering and nuclear engineering. This is mainly due to their several advantages compared to classical composites, namely, assuring continuous transition of stress distributions and reducing or removing of stress concentration, (Ghannad *et al.* 2012, Shaterzadeh and Foroutan 2016, Attia *et al.* 2018), Tu *et al.* 2017, Lee *et al.* 2017). Indeed, typical FGM plate-shell type structures are made of materials that are characterized by a continuous variation of the material properties over the thickness direction by mixing two different materials, (Denir *et al.* 2016, Bourada *et al.* 2015, Younsi *et al.* 2018).The most known FGMs are composed of transition alloys from metal at one surface to ceramic at the opposite surface, (Yang and Shena 2003, Woo and Merguid 2001, GhannadPour and Alinia 2006).Actually, the attractive physical and mechanical properties characterizing particulate reinforced metal matrix composites (MMCs) which combine metallic properties, such as ductility and toughness, with ceramic properties like high strength and high modulus, leading to greater strength in shear and compression and higher service temperature capabilities, have made them interesting candidate materials for aerospace, automotive, reactor vessels, and numerous other engineering applications, (Tjong and Ma 2000, El-Haina *et al*. 2017, Elmossouess *et al.* 2017, Barati *et al.* 2016, Bousahla *et al.* 2016, Frikha *et al*. 2016, 2017, 2018, Hajlaoui *et al.* 2017).

Due to increasing use of composite structures in advanced industries, it is crucial to apply an appropriate

*Corresponding author, Ph.D.
E-mail: hanen.j@gmail.com
[a]Ph.D.
E-mail: jamelmars@yahoo.fr
[b]Professor
E-mail: mondherwali@yahoo.fr
[c]Professor
E-mail: fakhreddine.dammak@enis.rnu.tn

ISSN: 1225-4568 (Print), 1598-6217 (Online)

theory in conjunction with a consistent and powerful numerical approach such as the finite element method. Three different approaches can be used to investigate the kinematics of these structures which are: the classical Kirchhoff-love theory (CST), the first-order shear deformation theory (FSDT) and the high-order-shear deformation theory (HSDT). The classical theory is adopted to model the kinematics of thin structures. This theory is simple to develop and allows results with reduced computational costs. However, the transverse shear deformation effect is ignored. Hence, the FSDT theory was proposed by Mindlin (1951) to include shear effects by using a constant shear coefficient (5/6 for isotropic materials). This model can be applied for both thin and moderately thick shell structures. Accordingly, the introduction of the HSDT theory allows to overcome the limitations of these models by considering a parabolic variation of the transverse shear strains across the shell thickness. This theory was developed by Reddy (1984) and it has already been used to analyze thick structures. However, the HSDT requires more kinematic variables and more computational time than those addressed above. Indeed, a comparative study between the FSDT and HSDT was provided by Shankara and Iyengar (1996) where they outlined that accurate results can be obtained from the FSDT theory for the analysis of laminated thick plates. Therefore, several finite element models have been developed to assure balance between computational efficiency and accuracy for global behaviour of composite structures. Civalek (2008) conducted a static analysis of thick symmetric cross-ply laminated composite plates based on FSDT. Using a finite element model based on the FSDT, free vibration, static and dynamic analysis of laminated composite plates and shells were performed in the works of (Gürses *et al.* 2009, Liew *et al.* 2004, Jin *et al.* 2013). Trabelsi *et al.* (2018) examined thermal post-buckling of functionally graded material shell structure. Further, an efficient hyperbolic shear deformation theory was proposed to investigate bending, buckling and free vibration of FGM sandwich and laminated composite plates by (Abdelaziz *et al.* 2017, Hebali *et al.* 2014, Mahi *et al.* 2015). In the same context, a refined trigonometric plate theory is provided in order to analyze hygro-thermo-mechanical bending (Beldjelili *et al.* 2016, Zidi *et al.* 2014), bending (Bouderba *et al.* 2016), buckling (Bellifa *et al.* 2017) and free vibration of FGM plates (Bellifa *et al.* 2016, Bennoun *et al.* 2016). Moreover, based on HSDT, several works were conducted to study the mechanical behavior of advanced composite plates taking into account linearity, nonlinearity and environmental effect (Bouhadra *et al.* 2018, Bousahla *et al.* 2014, Menasria *et al.* 2017). The HSDT is utilized by Zghal *et al.* (2017, 2018a, 2018b, 2018c) in order to investigate mechanical behavior of functionally graded carbon nanotube-reinforced plate and shell structures. Further, various numerical approximate methods for solving linear and nonlinear mechanical problems of composite material plate and shell are proposed such as: discrete singular convolution (DSC) method (Baltacıoglu *et al.* 2011, Civalek *et al.* 2013) and the differential quadrature (DQ) method (Talebitooti 2013). Several practical problems of FG structures require a geometrically non-linear formulation. However, it should be emphasized that analytical solutions of shell problems are very limited, (Hosseini Kordkheili and Naghdabadi 2012, Kar and Panda 2015) and most studies of the non-linear behavior of FGM plates and shells were limited to a von-Karman assumption taking into account plane stress only, which is restricted to moderately small deformations, Zhao and Liew (2009) and Phung-Van *et al.* (2014). Recently, Moita *et al.* (2016) conducted a static geometric and material nonlinear analysis for FGM plate-shell type structures. The formulation includes material and geometric nonlinearities and was implemented in a finite element model based on a non-conforming triangular flat plate/shell finite element in conjugation with the Reddy's third-order shear deformation theory.

On the other hand, material nonlinearity plays a major role in the behavior of FGM structures. Over the years, much research has been dedicated to describe the elastoplastic behavior of FGMs. In the open literature, the plasticity formulation follows generally a composite model proposed by Tamura *et al.* (1973), Tamura-Tomota-Ozawa model, referred as the TTO model, which is largely used to define the elastoplastic behavior of FGM structures, Williamson *et al.* (1993), Vaghefi *et al.* (2016) and Bocciarelli *et al.* (2008). According to the TTO model, the response is essentially directed by the plasticity dispersion in the metal phase. However, using this model, a stress transfer parameter, which depends on the constituent materials properties, have to be determined experimentally or/and numerically.

Elastoplastic static response of FGM shells undergoing large displacements and rotations is first investigated using ABAQUS software. Indeed, variations of the material properties in the transverse direction are often modeled in ABAQUS through the following method: dividing each layer into a sufficient number of slices to approximate the gradual variations of the material properties. Further, there is no need to change the mid-plane kinematics as all the coupling terms are considered especially the membrane-bending coupling terms.

The objective of this work is to introduce an alternative method based on FSDT to analyze the geometric non-linear static response of FG shells with elastoplastic properties. The material properties are introduced according to the integration points via the implementation of the user-material UMAT subroutine into ABAQUS software. The implementation is applicable to the analysis of elastoplastic functionally graded shells undergoing fully geometrically nonlinear mechanical response. The Mori-Tanaka model is employed in this present work to locally evaluate effective elastic parameters of the FGM composite and the self-consistent method of Suquet for the homogenization of the elastoplastic hardening law. The effectiveness of the developed material and geometric non-linear approach is evaluated through several non-trivial structure problems.

2. Formulation of non-linear elastoplastic FGM plate-shell problem

A description of the geometry and kinematics of

geometrically non-linear behavior of elastoplastic FGM plates-shells under mechanical loads is concisely provided in this section. Based on based on the First-order Shear Deformation Theory (FSDT), which accounts for the shear deformation effect by the way of a linear variation of in-plane displacements through the thickness, the present approach considers large deformations and finite rotations.

2.1 FG material properties

The proposed FGM plate-shell type structure is a particle reinforced metal matrix composite made by mixing two distinct material phases, namely an elastoplastic metal matrix reinforced by elastic ceramic particles. The material properties of a FGM plate-shell structures are assumed to vary continuously throughout the thickness direction (z-axis direction), according to a power function of the volume fractions of the constituents. Based on the power-law model employed by Bao and Wang (1995), the volume fraction of the ceramic phase V_c can be considered as below

$$V_c(z)=\left(\frac{z}{h}+\frac{1}{2}\right)^p \quad ; \quad V_c(z)+V_m(z)=1 \tag{1}$$

where $z \in [-h/2; h/2]$, h is the thickness of the structure, and the exponent p is the nonnegative power-law index which determines gradation of material properties across the thickness direction. The subscripts m and c denote metal and ceramic, respectively.

To describe the elastic proprieties of the FGM shells, the rule of mixtures approach is generally used, however, it does not account for the interaction between particle phases. In order to overcome this limitation, Mori-Tanaka model is employed in many studies for underlying micromechanics and homogenization of particle reinforced Metal Matrix Composites, Rahman and Chakraborty (2007), Pettermann (2010), Yu and Kidane (2014). In this study, Mori-Tanaka model is used to reliably predicting the effective elastic proprieties of two-phase solid composites based on the input of the individual properties of the phases.

The homogenized Poisson's ratio and Young's modulus at each single point through the thickness direction are given by

$$\nu(z)=\frac{1}{2}\frac{3k(z)-2G(z)}{3k(z)+G(z)} \quad ; \quad E(z)=2G(z)(1+\nu(z)) \tag{2}$$

where the effective bulk modulus $k(z)$ and the effective shear modulus $G(z)$ of the components are defined according to Mori-Tanaka method as follows

$$k(z)=k_m\frac{1+V_c\left(\frac{k_c}{a_1k_m}-1\right)}{1+V_c\left(\frac{1}{a_1}-1\right)} \quad ; \quad a_1=1+\frac{(1+\nu_m)}{3(1-\nu_m)}\left(\frac{k_c}{k_m}-1\right) \tag{3}$$

$$G(z)=G_m\frac{1+V_c\left(\frac{G_c}{b_1G_m}-1\right)}{1+V_c\left(\frac{1}{b_1}-1\right)} \quad ; \quad b_1=1+\frac{2(4-5\nu_m)}{15(1-\nu_m)}\left(\frac{G_c}{G_m}-1\right) \tag{4}$$

2.2 Kinematics of non-linear FGM plate-shell structures

In this section, the geometry and kinematic of the non-linear shell model are depicted. The shell's geometry in the 3D space is described in a global Cartesian coordinate system. Initial and current configurations of the shell, are designated, respectively, by C_0 and C_t. Associated variables with the undeformed state C_0 will be symbolized by upper-case letters and by a lower-case letters when referred to the deformed configuration C_t. Vectors will be denoted by bold letters.

All material point of the shell are defined using parameterizations in terms of curvilinear coordinates $\boldsymbol{\xi}=\left(\xi^1,\xi^2,\xi^3=z\right)$. The pair ($\boldsymbol{X}_p$, $\boldsymbol{D}$) defines the position of an arbitrary point 'q' of the shell. $\boldsymbol{X}_p$ gives the position of a point 'p' on the shell midsurface. The reference surface of the shell is assumed to be smooth, continuous and differentiable. **D** is a director unit vector and h is the thickness of the element. The position vector $\underline{\boldsymbol{X}}_q$ in $\boldsymbol{C}_0$, is defined as following

$$\boldsymbol{X}_q\left(\xi^1,\xi^2,z\right)=\boldsymbol{X}_p\left(\xi^1,\xi^2\right)+z\,\boldsymbol{D}\left(\xi^1,\xi^2\right) \quad ; z\in\left[-\frac{h}{2},\frac{h}{2}\right] \tag{5}$$

Considering the hypothesis of first order shear deformation theory (FSDT), the position vector of the point 'q' in the deformed configuration C_t is given by

$$\boldsymbol{x}_q\left(\xi^1,\xi^2,z\right)=\boldsymbol{x}_p\left(\xi^1,\xi^2\right)+z\,\lambda\,\boldsymbol{d}\left(\xi^1,\xi^2\right) \quad ; z\in\left[-\frac{h}{2},\frac{h}{2}\right] \tag{6}$$

where $\boldsymbol{d}$ is the director vectors of the deformed configurations and λ is the stretching parameter which depends on the actual state of deformation gradient and evaluated in the mid-surface (z=0).

The strain tensor can be decomposed in-plane and transverse shear strains as given by

$$\begin{cases}\varepsilon_{\alpha\beta}=e_{\alpha\beta}+z\,\lambda\,\chi_{\alpha\beta} & ;\alpha,\beta=1,2\\ \gamma_{\alpha3}=\boldsymbol{a}_\alpha.\boldsymbol{d}\end{cases} \tag{7}$$

in which $(a_\alpha),\alpha=1,2$ are the local orthonormal shell direction in deformed state and $\gamma_{\alpha3}$, $e_{\alpha\beta}$ and $\chi_{\alpha\beta}$ denote respectively transverse shear, membrane and bending strains. Membrane $e_{\alpha\beta}$ and bending $\chi_{\alpha\beta}$ strains can be expressed as

$$e_{\alpha\beta}=\frac{1}{2}\left(a_{\alpha\beta}-A_{\alpha\beta}\right) \quad ; \quad \chi_{\alpha\beta}=\frac{1}{2}\left(b_{\alpha\beta}-B_{\alpha\beta}\right) \quad ;\alpha,\beta=1,2 \tag{8}$$

where $A_{\alpha\beta}$ and $a_{\alpha\beta}$ are metric tensors in the reference and deformed configuration, respectively, and they are given by

$$A_{\alpha\beta}=\boldsymbol{X}_{p,\alpha}.\boldsymbol{X}_{p,\beta} \quad ; \quad a_{\alpha\beta}=\boldsymbol{x}_{p,\alpha}.\boldsymbol{x}_{p,\beta} \quad ;\alpha,\beta=1,2 \tag{9}$$

in which the notation $(.)_{,\alpha}=\partial(.)/\partial S^\alpha$ is used. $B_{\alpha\beta}$ and $b_{\alpha\beta}$ are the curvature tensors in the reference and deformed configuration, respectively, and they are given by

$$B_{\alpha\beta}=\boldsymbol{X}_{p,\alpha}.\boldsymbol{D}_{,\beta}+\boldsymbol{X}_{p,\beta}.\boldsymbol{D}_{,\alpha} \quad ; \quad b_{\alpha\beta}=\boldsymbol{x}_{p,\alpha}.\boldsymbol{d}_{,\beta}+\boldsymbol{x}_{p,\beta}.\boldsymbol{d}_{,\alpha} \quad ;\alpha,\beta=1,2 \tag{10}$$

The membrane $\boldsymbol{e}$, bending $\boldsymbol{\chi}$ and shear $\boldsymbol{\gamma}$ strains vectors are expressed in matrix form by

$$\boldsymbol{e}=\begin{bmatrix} e_{11} \\ e_{22} \\ 2e_{12} \end{bmatrix} \quad ; \quad \boldsymbol{\chi}=\begin{bmatrix} \chi_{11} \\ \chi_{22} \\ 2\chi_{12} \end{bmatrix} \quad ; \quad \boldsymbol{\gamma}=\begin{bmatrix} \gamma_{13} \\ \gamma_{23} \end{bmatrix} \tag{11}$$

In matrix form, the membrane $\boldsymbol{N}$, bending $\boldsymbol{M}$ and shear $\boldsymbol{T}$ generalized internal forces, can be expressed, respectively, as

$$\boldsymbol{N}=\int_{-h/2}^{h/2}\begin{bmatrix} \sigma_{11} \\ \sigma_{22} \\ \sigma_{12} \end{bmatrix} dz \quad ; \quad \boldsymbol{M}=\int_{-h/2}^{h/2} \lambda z \begin{bmatrix} \sigma_{11} \\ \sigma_{22} \\ \sigma_{12} \end{bmatrix} dz \quad ; \quad \boldsymbol{T}=\int_{-h/2}^{h/2}\begin{bmatrix} \sigma_{13} \\ \sigma_{23} \end{bmatrix} dz \tag{12}$$

where σ_{ij} are the components of stress tensor. Consequently, the resultants stress and strain fields given in Eqs. (11) and Eqs. (12) can be arranged to form the generalized resultant stress $\boldsymbol{R}$ and generalized strain $\boldsymbol{\Sigma}$ as

$$\boldsymbol{R}=\begin{bmatrix} \boldsymbol{N} \\ \boldsymbol{M} \\ \boldsymbol{T} \end{bmatrix} \quad ; \qquad \boldsymbol{\Sigma}=\begin{bmatrix} \boldsymbol{e} \\ \boldsymbol{\chi} \\ \boldsymbol{\gamma} \end{bmatrix} \tag{13}$$

For a FGM elastic shell, the Generalized Hook's Law allows for the following relations between strains and stresses

$$\boldsymbol{R}=\boldsymbol{H}_T\,\boldsymbol{\Sigma} \quad , \qquad \boldsymbol{H}_T=\begin{bmatrix} \boldsymbol{H}_m & \boldsymbol{H}_{mb} & 0 \\ \boldsymbol{H}_{mb} & \boldsymbol{H}_{bb} & 0 \\ 0 & 0 & \boldsymbol{H}_s \end{bmatrix} \tag{14}$$

where

$$\begin{cases} \left(\boldsymbol{H}_m,\, \boldsymbol{H}_{mb},\, \boldsymbol{H}_{bb}\right)=\int_{-h/2}^{h/2}\left(1, z, z^2\right)\boldsymbol{H}_\pi \, dz \\ \boldsymbol{H}_s=\boldsymbol{K}\odot\int_{-h/2}^{h/2}\boldsymbol{H}_\eta \, dz \end{cases} \tag{15}$$

in which $\boldsymbol{H}_\pi$ and $\boldsymbol{H}_\eta$ are, respectively, the in plane and out-of-plane linear elastic sub-matrices which components contain material properties, given by

$$\boldsymbol{H}_\pi=\frac{E(z)}{1-\nu^2(z)}\begin{bmatrix} 1 & \nu(z) & 0 \\ \nu(z) & 1 & 0 \\ 0 & 0 & (1-\nu(z))/2 \end{bmatrix}, \quad \boldsymbol{H}_\eta=\frac{E(z)}{2(1+\nu(z))}\begin{bmatrix} 1 & 0 \\ 0 & 1 \end{bmatrix} \tag{16}$$

where $E(z)$ and $\nu(z)$ are the Young's modulus and the Poisson's ratio respectively. In Eq. (15), $\mathbf{k}$ is the shear correction matrix computed based on the work of Hajlaoui *et al.* (2015).

2.3 Elastoplastic stress–strain relation of FGM plate-shell structures

In this part, the elastoplastic formulation of ceramic/metal FGM shell is briefly described. Plasticity models are formulated in terms of the yield surface, the flow rule and the homogenized evolution laws that define the hardening of the particle reinforced Metal Matrix Composites. A self-consistent model is adopted to evaluate effective elastoplastic parameters of the ceramic/metal FGM composite.

The elastoplastic behaviour can be described as follows: materials present an elastic behaviour until the yield stress, is achieved, beyond this point, the material start to exhibit plastic behaviour and the relation between stress and strain is obtained by a tangent modulus.

Before the material gets in the plastic state, Hooke's law Eq. (14) describes the relation between stress and strain. However, after the material surpasses the stress level set by the yield criterion, Hooke's law is no longer efficient, and the stress state progresses with respect to a plastic flow rule. Plastic behaviour is noticeable when there are irreversible strains on the solid after the load is eliminated. Taking into account of constant volume deformations associated to this behaviour, elastic and plastic strain components can be additively decomposed as

$$\boldsymbol{\varepsilon}=\boldsymbol{\varepsilon}^e+\boldsymbol{\varepsilon}^p \tag{17}$$

where $\boldsymbol{\varepsilon}^e$ represents the elastic component of strain and $\boldsymbol{\varepsilon}^p$ the plastic one.

The following relation between the stress rate and the strain rate, can be assumed

$$\dot{\boldsymbol{\sigma}}=\boldsymbol{H}\,\dot{\boldsymbol{\varepsilon}}^e=\boldsymbol{H}\left(\dot{\boldsymbol{\varepsilon}}-\dot{\boldsymbol{\varepsilon}}^p\right) \tag{18}$$

where $\boldsymbol{H}$ is the general elastic operator (the fourth order material constitutive tensor).

During plastic deformation, the yield surface can be described by

$$f\left(\boldsymbol{\sigma},\kappa\right)=\varphi\left(\boldsymbol{\sigma}\right)-\sigma_p\left(\kappa\right)=0 \quad , \sigma_p\left(\kappa\right)=\sigma_Y+R\left(\kappa\right) \tag{19}$$

where σ_Y is the yield stress, R represents the drag stress in isotropic hardening and κ is the internal variable corresponding to isotropic hardening. From the Von-Mises J_2 criterion, for the case of an isotropic material the function $\varphi\left(\boldsymbol{\sigma}\right)$ is the equivalent stress, which may be written as, Belhassen *et al.* (2016, 2017)

$$\varphi(\boldsymbol{\sigma})=\|\boldsymbol{\sigma}\|_{\boldsymbol{Q}}=\sqrt{\boldsymbol{\sigma}^T\boldsymbol{Q}\,\boldsymbol{\sigma}} \qquad \text{where } [\boldsymbol{Q}]=\begin{bmatrix} 1 & -0.5 & -0.5 & 0 & 0 & 0 \\ & 1 & -0.5 & 0 & 0 & 0 \\ & & 1 & 0 & 0 & 0 \\ & & & 3 & 0 & 0 \\ & Sym & & & 3 & 0 \\ & & & & & 3 \end{bmatrix} \tag{20}$$

It can be noted that constitutive relations of the elastoplastic material are given in terms of the rates of stress and strain. Accordingly, the evolution equations for the present problem are given as follows

$$\dot{\boldsymbol{\varepsilon}}^p=\dot{\gamma}\frac{\partial f}{\partial \boldsymbol{\sigma}}=\dot{\gamma}\,\boldsymbol{n} \quad ; \qquad \boldsymbol{n}=\frac{1}{\varphi}\boldsymbol{Q}\boldsymbol{\sigma} \tag{21}$$

$$\dot{\kappa}=-\dot{\gamma}\frac{\partial f}{\partial R}=\dot{\gamma} \tag{22}$$

The plastic strain rate is defined as proportional to the stress gradient of a plastic potential, which is taken equal to the yield surface condition *f* for an associated flow rule. $\boldsymbol{n}$ is the flow vector which defines direction of the plastic strain increment to be perpendicular to the yield surface and $\dot{\gamma}$ is the plastic multiplier which is consistent with the loading/unloading conditions given by

$$\dot{\gamma} \geq 0\,; \quad f \leq 0\,; \quad \dot{\gamma} f = 0 \tag{23}$$

The description of how the yield surface changes with plastic deformation is called the hardening law. Ceramic materials are, commonly, brittle materials of almost greater elastic modulus and strength than those of metallic materials, which have generally ductile properties. Therefore, the ceramic particles in FGM are assumed to have linear elastic behavior when deformation takes place. The elastoplastic deformation occurs primarily by the plastic flowing of the metallic matrix phase. In the present study, the behavior of the matrix phase, the metal, is assumed to be elastoplastic with isotropic hardening according to the power plastic hardening law of Ludwik, Gunes *et al.* (2014).

$$\sigma_m = \sigma_{Ym} + K_m r^{n_m} \tag{24}$$

in which $\sigma_m\left(MPa\right)$ is the stress, $\sigma_{Ym}\left(MPa\right)$ is the yield strength, r is the plastic strain, n_m is the strain hardening exponent and $k_m(Mpa)$ is the strength coefficient corresponding to the metal. To depict the elastic-plastic behavior of ceramic/metal composite, the same hardening law of Ludwik is adopted for the FGM shells.

$$\sigma_p = \sigma_Y + K r^n \tag{25}$$

Where $\sigma_Y\left(MPa\right)$ is the effective yield strength, n is effective strain hardening exponent and $K(MPa)$ is the effective strength coefficient corresponding to the ceramic/metal FGM shell.

To improve the description of elastoplastic behavior of ceramic/metal FGM, an asymptotic homogenization algorithm was developed by Orlik (2010), to characterize elastoplastic composites with pure elastic inclusions and elastoplastic metallic matrix using Ludwik hardening law. The asymptotic homogenization method was performed using ABAQUS software, in Orlik (2010) study, for obtaining effective material properties of a reinforced metal-matrix elastoplastic composite involving a 10% volume fraction of arbitrarily located ball-shaped inclusions with normally distributed radius. The effective properties computed by the asymptotic approach closely matched those obtained from experiments and those determined by Suquet self-consistent formulas. However, such an approach requires complex computer simulations and would be extremely time-consuming and very costly. Alternatively, self-consistent formulas, like Hashin, Eshelby and Suquet models are used, due to their simplicity. Suquet self-consistent formulas proved to be useful to accurately estimate effective properties of particulate composites with low to moderate volume fractions of inclusions and for composites with granular microstructures, Suquet (1997). Accordingly, effective elastoplastic parameters of the ceramic/metal FGM shell, σ_Y, K and n, are calculated, in the present work, by the homogenization and averaging formulas of Suquet (1997)

$$\sigma_Y = \frac{E}{E_m}\sigma_{Ym} \quad ; \quad K = K_m \frac{1+V_c}{\left(1-V_c\right)^n} \quad ; \quad n = n_m \tag{26}$$

2.4 Weak form and linearization:

This kinematic constraint will be imposed in a discrete form in the finite element approximation. Now consider the internal virtual work

$$W_{int} = \int_V \sigma_{ij}\delta\varepsilon_{ij} dV = \int_V \left[\sigma_{\alpha\beta}\left(\delta e_{\alpha\beta} + z\lambda\delta\chi_{\alpha\beta}\right) + \sigma_{\alpha 3}\delta\gamma_{\alpha 3}\right] dV \tag{27}$$

where dV is the shell volume element in the initial configuration, $\delta\varepsilon_{ij}$ is the virtual strain tensor and σ_{ij} the components of the stress tensor.

Inserting the membrane, bending and shear stress resultants $\boldsymbol{N}$, $\boldsymbol{M}$ and $\boldsymbol{T}$ respectively given by Eq. (12) and the shell strains $\delta\mathbf{e}$, $\delta\boldsymbol{\chi}$ and $\delta\boldsymbol{\gamma}$ represented in Eq. (11) into Eq. (27) and integrating through the thickness of the shell, the weak form can be rewritten as

$$W = \int_A \left(\delta\boldsymbol{e}.\boldsymbol{N} + \delta\boldsymbol{\chi}.\boldsymbol{M} + \delta\boldsymbol{\gamma}.\boldsymbol{T}\right) dA - W_{ext} = 0 \tag{28}$$

where W_{ext} is the external virtual work.

In order to describe the non-linear shell problem, the weak form of the equilibrium equation, Eq. (28), can be rewritten as a function of the nodal displacement vector $\boldsymbol{U_n}$ involving the generalized resultant stress $\boldsymbol{R}$ and generalized strain $\boldsymbol{\Sigma}$ as follows

$$W\left(\boldsymbol{U}_n\right) = \int_A \delta\boldsymbol{\Sigma}^T.\boldsymbol{R}\, dA - W_{ext}\left(\boldsymbol{U}_n\right) = 0 \tag{29}$$

The Eq. (29), is solved iteratively with the Newton-Raphson algorithm. Indeed, the consistent tangent operator, needed to ensure the quadratic convergence of global Newton-Raphson approach, is built up by providing the directional derivative of the weak form in the direction of the increment $\Delta\boldsymbol{U}_n$. The tangent operator is decomposed, in a straight practice, into material and geometric parts as follows

$$\Delta W_{\text{int}} = \delta\boldsymbol{U}_n^T\left(\boldsymbol{K}_M + \boldsymbol{K}_G\right)\Delta\boldsymbol{U}_n \tag{30}$$

in which $\boldsymbol{K}_M$ and $\boldsymbol{K}_G$ designate, respectively, material and geometric stiffness matrices. In fact, the geometric part $\boldsymbol{K}_G$ of the tangent operator, originates from the variation of the virtual strains while keeping stress resultant fixed, whereas, the material part $\boldsymbol{K}_M$ of the tangent operator, issues from the variation in the stress resultants while maintaining virtual strains unchanged.

3. Numerical implementation

A user defined subroutine (UMAT) is developed and

implemented in Abaqus/Standard to study the elastoplastic behavior of the ceramic particle-reinforced metal-matrix FGM plates-shells undergoing large displacements and rotations.

3.1 Elastoplastic numerical integration scheme

The elastoplastic response of the studied ceramic/metal FGM shell is simulated using Abaqus/Standard "incremental" theories. Iterative plasticity models are formulated in terms of the yield surface, the flow rule and the homogenized evolution laws that define the hardening of the metal/ceramic FGM structure. It can be noted that constitutive relations of the elastoplastic material are given in terms of the rates of stress and strain (Eq. (18)). Elastic and plastic strains are separated because unique elastic strain generates stress which can only be calculated by integrating the stress rate over the past load history. The integration is conducted using the implicit Euler method (Backward Euler method), the strain-driven integration algorithm allows to have the stress history from the strain history.

The plastic strain $\boldsymbol{\varepsilon}_{n+1}^{p}$ are determined by integration of the flow rule over a time step using the implicit backward Euler's method which makes the algorithm unconditionally stable, which lead to

$$\boldsymbol{\varepsilon}_{n+1}^{p}=\boldsymbol{\varepsilon}_{n}^{p}+\Delta\gamma\ \boldsymbol{n}_{n+1} \quad ; \quad \boldsymbol{n}_{n+1}=\frac{1}{\varphi_{n+1}}\boldsymbol{Q}\boldsymbol{\sigma}_{n+1} \tag{31}$$

Using the decomposition of strain, Eq. (17) and the elasticity relation, Eq. (18), the stress tensor can be written as

$$\boldsymbol{\sigma}_{n+1}=\boldsymbol{H}\left(\boldsymbol{\varepsilon}_{n+1}-\boldsymbol{\varepsilon}_{n+1}^{p}\right)=\boldsymbol{\sigma}^{trial}-\sqrt{3/2}\,\Delta\gamma\boldsymbol{H}.\boldsymbol{n}_{n+1} \tag{32}$$

where $\boldsymbol{\sigma}^{trial}$ is the elastic trial stress

$$\boldsymbol{\sigma}^{trial}=\boldsymbol{\sigma}_{n}+\boldsymbol{H}\Delta\boldsymbol{\varepsilon} \tag{33}$$

Using Eqs. (31) and (32), the stress tensor, $\boldsymbol{\sigma}_{n+1}$, can then be computed as

$$\boldsymbol{\sigma}_{n+1}=\boldsymbol{I}_{c}^{-1}.\boldsymbol{\sigma}^{trial} \quad ; \quad \boldsymbol{I}_{c}=\boldsymbol{I}+u\,\boldsymbol{H}\boldsymbol{Q} \quad ; \quad u=\frac{\Delta\gamma}{\varphi_{n+1}} \tag{34}$$

From Eqs. (19) and Eqs. (34), it follows that the enforcement of the consistency condition is reduced to one scalar equation. The unknown of this equation is the plastic multiplier $\Delta\gamma$. This equation is solved using the Newton method.

$$f(\Delta\gamma)=\varphi-(\sigma_{Y}+R)=0 \quad ; \quad \varphi=\left[\boldsymbol{\sigma}^{trial\,T}.\boldsymbol{I}_{c}^{-T}.\boldsymbol{Q}.\boldsymbol{I}_{c}^{-1}.\boldsymbol{\sigma}^{trial}\right]^{1/2} \tag{35}$$

One step of the incremental and iterative numerical solution algorithm using the Newton-Raphson iteration applied to solve Eq. (35) is summarized in Box 1.

With this integration procedure, it is essential to use the algorithmic tangent modulus in order to preserve the quadratic rate of asymptotic convergence of Newton

Box 1: Integration algorithm

Set : $\Delta\gamma=0$

(I) Compute trial elastic stress

$\boldsymbol{\sigma}^{trial}=\boldsymbol{H}\left(\boldsymbol{\varepsilon}_{n+1}-\boldsymbol{\varepsilon}_{n}^{p}\right)$

(II) Find $\Delta\gamma$ by local iteration k

(i) $f_k=\varphi_k-\sigma_{p,k}$, $\varphi_k=\left[\boldsymbol{\sigma}^{trial\,T}.\boldsymbol{I}_{c}^{-T}.\boldsymbol{Q}.\boldsymbol{I}_{c}^{-1}.\boldsymbol{\sigma}^{trial}\right]^{1/2}$

$\boldsymbol{I}_{c}=\boldsymbol{I}+u\,\boldsymbol{H}\boldsymbol{Q}$, $u=\frac{\Delta\gamma}{\varphi_k}$

(ii) $f_k^{'}=\frac{d\varphi_k}{d(\Delta\gamma)}-\sigma_{p,k}^{'}$

(iii) $\Delta\gamma_{k+1}=\Delta\gamma_k-\frac{f_k}{f_k^{'}}$

(iv) if $|f_k|>Tol$ then $k=k+1$ go to (i)

(III) Update variables

$\boldsymbol{\sigma}_{n+1}=\boldsymbol{I}_{c}^{-1}.\boldsymbol{\sigma}^{tr}$

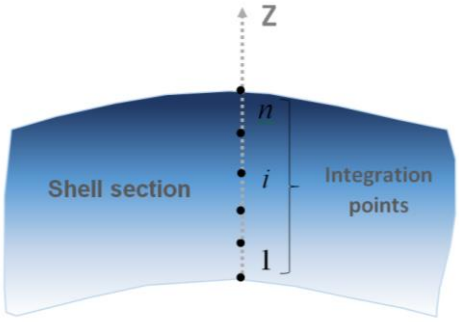

Fig. 1 Simpson's approach for integration through the thickness of the FGM shell

method. Using this integration method, an algorithmic tangent modulus is employed to maintain the quadratic rate of asymptotic convergence of the Newton approach used to determine the plastic multiplier as detailed in the works of Belhassen *et al.* (2016), Wali *et al.* (2015, 2016), Mars *et al.* (2016, 2017), Ben Said *et al.* (2017) and Autay *et al.* (2017).

3.2 Through-thickness integration and UMAT interface

The standard quadrilateral 4-nodes shell element with three rotational and three translational degrees of freedom per node, S4, is extended in the present study, to deal with elasto-plastic analysis of geometrically non-linear ceramic/metal FGM plate-shell structures. The elastoplastic material properties are assumed to vary smoothly through the thickness of the plate-shell type structures. Numerical integration through the thickness of shell elements is needed to compute resultant stress and the consistent tangent operator from. To avoid stress discontinuity at the interfaces, a UMAT subroutine is implemented into ABAQUS in order to define the material properties according to the coordinates of the integration points. It should be noted that two kinds of numerical integration may be used: Gauss and Simpson integration. To obtain an accurate analysis of FGM structure using shell elements, the number of the through-thickness integration points (n) should be carefully chosen, since a small number of integration points can create an additional error of the numerical results.

In ABAQUS the integration points through the thickness

Box 2 Material and geometric nonlinear analysis methodology using UMAT subroutine implemented into ABAQUS

Input elasto-plastic material proprieties $E_m, \nu_m, E_c, \nu_c, \sigma_{Ym}, K_m$ and n_m

Loop over thickness points integration
Call UMAT(….DDSDDE, STRESS, KSPT, PROPS…)

- Computation parametric coordinate (ξ_{KSPT}): $-1 \le \xi_{KSPT} \le 1$
- Computation of reel coordinate (Z_{KSPT}): $\frac{-h}{2} \le Z_{KSPT} \le \frac{h}{2}$
- Homogenization and computation of effective elastoplastic parameters E, σ_Y, K and n : PROPS (Z_{KSPT})
- Computation of consistent tangent operator of elastoplastic behaviour: DDSDDE (Z_{KSPT})
- Computation of stress tensor: STRESS (Z_{KSPT})

Element Stiffness matrix is obtained through-thickness integration

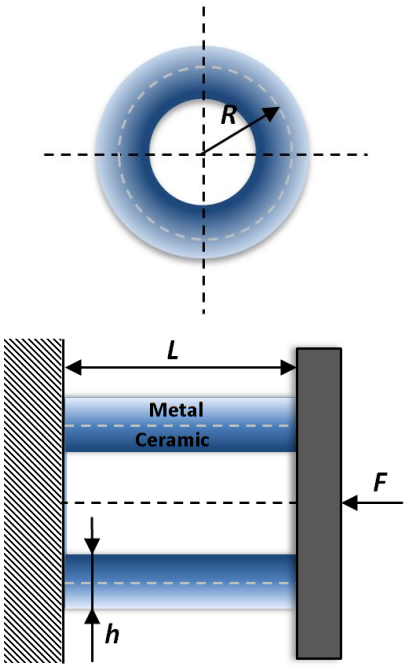

Fig. 2 Geometry of axially loaded FGM cylindrical shells

of the FGM shell are counted consecutively, starting with point (1) to point (n). Considering Simpson's approach, point (1) is situated exactly on the bottom surface of the shell, as illustrated in Fig. 1 and using Gauss quadrature, point (1) is located near to the bottom surface, more details can be found in ABAQUS documentation.

Numerical study is conducted using the UMAT subroutine implemented into ABAQUS. It should be mentioned that for each integration point through the thickness of the shell using the integration point number (KSPT), ABAQUS make a call for the UMAT subroutine. Box 2 provides better explanation of material and geometric nonlinear analysis methodology.

4. Numerical results and discussion

4.1 Validation results

The present work focus on material and geometrically non-linear behavior of elastoplastic functionally graded shells using ABAQUS. To ensure the validity of the present method, comparisons are performed with experimental and numerical solutions from the literature.

Table 1 Comparison of deflections results of axially compressed elastoplastic FGM cylindrical shells, h=0.4 mm

Axial Forces (kN)	Displacements (mm)	
	Xu *et al.* (2017)	Present method
0	0	0
5	0.02095	0.02122
10	0.04112	0.03988
15	0.06959	0.06856
30	0.10159	0.09928
40	0.18351	0.18602
50	0.24752	0.23954

Table 2 Mechanical properties of aluminum Al and SiC materials, Gunes *et al.* (2014)

Materials	Young modulus (GPa)	Poisson's ratio
Al 6061	67	0.33
SiC	302	0.17

Xu *et al.* (2017) have been numerically investigating the postbuckling of axial compressed elastoplastic functionally graded cylindrical shells. The FGM cylindrical shells are assumed to be simply supported at both ends, with thickness h, length L=100 mm, and mean radius R=50 mm, are subjected to uniform axial compression force F as shown in Fig. 2. The elastoplastic material properties are assumed to be multi-linear hardening type according to the constituent distributions and depicted by the TTO homogenized mixture rule, Xu *et al.* (2017).

The basic parameters in this example are chosen according to Xu *et al.* (2017): TiB/Ti FGMs with the material properties E_c=375 GPa, ν_c=0.14, E_m=107 GPa, ν_c=0.34, σ_{Ym}=450 MPa.

To verify the present FE model, buckling deformations results of axially compressed elastoplastic FGM cylindrical shells are compared with those obtained by Xu *et al.* (2017). Table 1 reports elastoplastic deflections of axially compressed FGM cylindrical shell acquired using the present and Xu *et al.* (2017) solutions. As may be seen, using both solutions the deflection in the postbuckling state enlarges with the increase of axial compression displacement.

From Table 1, the present results are well consistent with numerical solution of Xu *et al.* (2017), there are slight differences between both solutions, which is reasonable because two different homogenization approaches are used. Indeed, the Mori-Tanaka model and self-consistent formulas of Suquet are employed in this present work, whereas, Xu *et al.* (2017) used the TTO homogenized mixture rule.

The response of ceramic/metal FGM shells taken into accounts both material and geometric nonlinearities is investigated in this work. The studied FGM shell is a

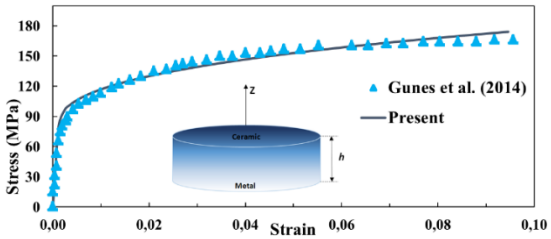

Fig. 3 True stress-strain curve of the aluminum as constituent in the circular FGM plates

Table 3 Elastoplastic properties of the Al 6061 material

Materials	$\sigma_{Ym}(MPa)$	$K_m(MPa)$	n_m
Al 6061	80	237.33	0.3878

particle reinforced metal matrix composite made by mixing two distinct material phases, namely an elastoplastic metal matrix of aluminum alloy (Al 6061) reinforced by elastic ceramic particles of silicon carbide (SiC). The mechanical properties of aluminum Al and SiC are given in Table 2.

Gunes *et al.* (2014) investigated experimentally and numerically low-velocity impact behaviour of functionally graded clamped circular plates composed of ceramic (SiC) and metal (Al) phases varying through the plate thickness. In order to describe the elastoplastic characteristics of metal/ceramic FGMs the TTO law of mixture was used in Gunes *et al.* (2014). A clamped FGM circular plate impacted at its center by a cylindrical impactor with hemispherical nose is considered. The circular Al/SiC FGM plate has 50 mm in diameter and 10 mm in thickness. This FGM plate is fixed by an annular support with an internal diameter of 40 mm, see Gunes *et al.* (2014).

In the present work, the behavior of the matrix phase, the aluminum alloy (Al 6061), is assumed to be elastoplastic with isotropic hardening according to plastic hardening law of Ludwik. Parameters (σ_{Ym}, K_m, n_m) required for Ludwik law can be determined by fitting experimentally measured data obtained by Gunes *et al.* (2014) according to Eq. (24). The Levenberg-Marquardt approach is applied to solve these non-linear least squares minimization problem. The final parameters of Ludwik hardening law for the aluminum phase, needed for the homogenization and averaging formulas of Suquet (1997), Eq. (26), are given in Table 3. Fig. 3 depicts the true stress-strain curve of the Al 6061 material, experimentally given in the work of Gunes *et al.* (2014) and numerically based on Ludwik hardening law.

To the best of the authors' knowledge, no relevant theoretical approach and experimental research has been presented for the elastoplastic analysis of FGM plates and shells, due to the difficulties in theoretically considering of both the material and geometrical nonlinearities.

To check the effectiveness of the developed model, the variation of contact force for Al/SiC FGM circular plates through time under impact velocity of 1.59 m/s and for power law index p=0.1 is compared to experimental and numerical results obtained by Gunes *et al.* (2014).

As may be seen in Fig. 4, results obtained by the current

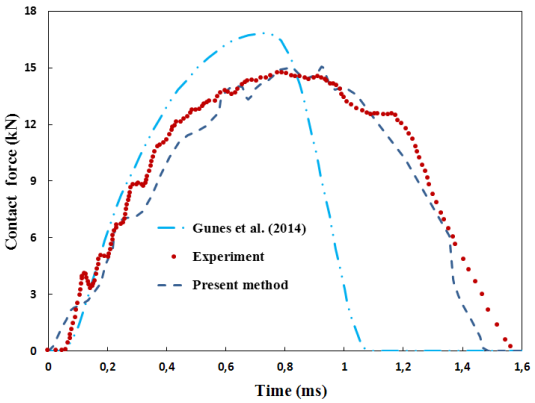

Fig. 4 Comparison of the the variation of contact force for Al/SiC FGM circular plates through time under impact velocity of 1.59 m/s and for power law index p=0.1

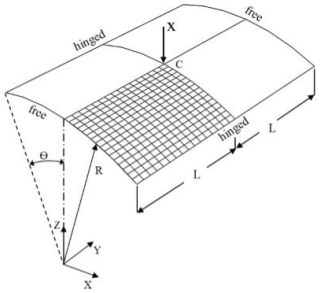

Fig. 5 Hinged FGM cylindrical roof subjected to a concentrated load

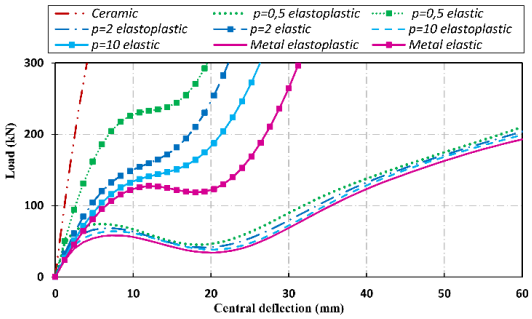

Fig. 6 Elastoplastic and elastic Load-deflection curves of the hinged cylindrical roof, h=20 *mm*

approach are in good agreement with those acquired in Gunes *et al.* (2014). It can be noticed that the present solution is closer to the experimental results compared to the numerical solution proposed by Gunes *et al.* (2014). This is principally due to the different homogenization methods employed in simulations. The current formulation is based on the Mori-Tanaka model and self-consistent formulas of Suquet, while, the TTO law of mixture was used by Gunes *et al.* (2014), which proves clearly that the Mori-Tanaka model and self-consistent formulas of Suquet allow better description of the elastoplastic characteristics of metal/ceramic FGMs.

4.2 Numerical examples

In order to demonstrate the robustness of the developed

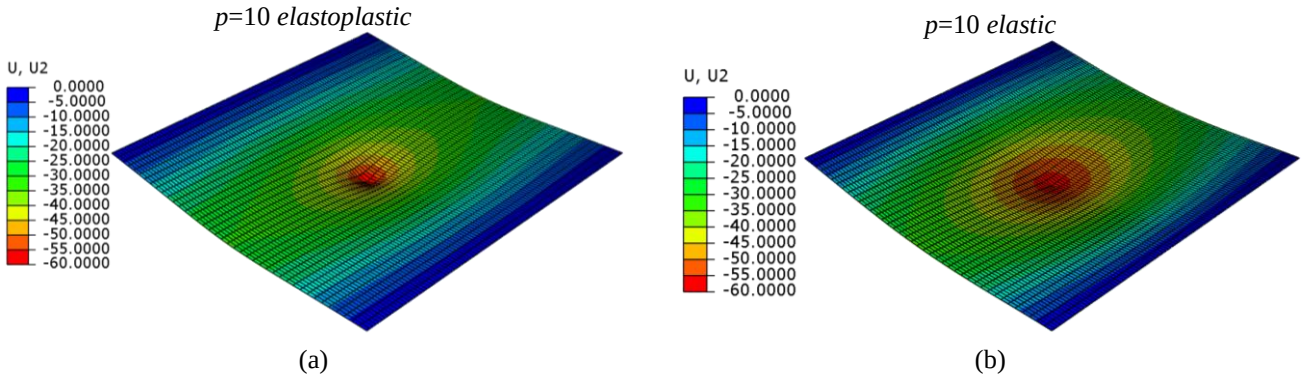

(a) (b)

Fig. 7 Elastoplastic and elastic deformed shapes of the hinged FGM cylindrical roof subjected to central displacement, for power law index p=10, U2: radial displacement and h=20 *mm*

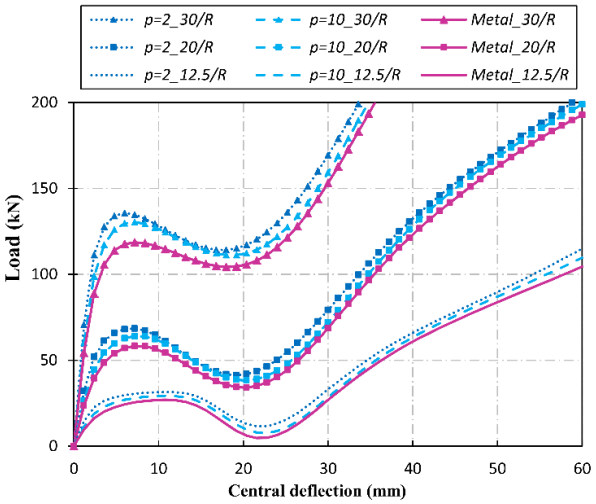

Fig. 8 Effect of the slenderness ratio h/R on load- deflection curves of the hinged cylindrical roof

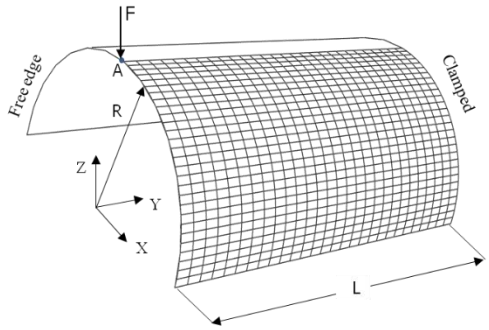

Fig. 9 Geometry of the semi-cylindrical FGM shell subjected to a pinching force

formulation and the performance of the finite element implementation, numerical examples of non-trivial benchmark problems taken from the literature are presented. Numerical simulations are conducted using the UMAT subroutine implemented into ABAQUS. The implementation is applicable to the analysis of functionally graded shells undergoing coupled material and geometrically nonlinear mechanical response. We focus on applications with warped elements and on the finite rotation capability. The standard quadrilateral 4-nodes shell element

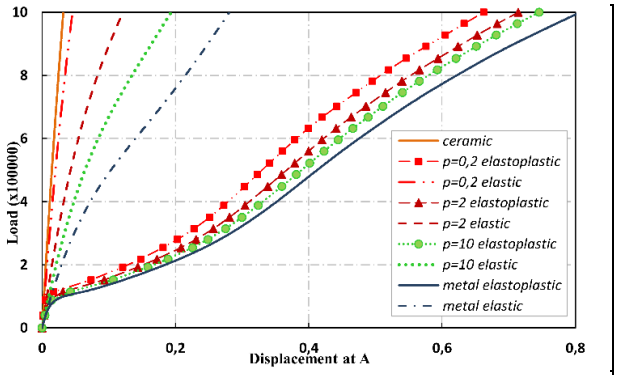

Fig. 10 Elastic and elastoplastic load-deflection curves of the pinched FGM cylindrical shell at A

with three rotational and three translational degrees of freedom per node, S4, is used to model all proposed geometries. Based on FSDT, the shell formulation of this element is derived using finite-membrane strain, which makes it suitable for modeling thin to moderately thick shell structures.

4.2.1 Hinged cylindrical roof subjected to central displacement

The first example considers a FG cylindrical shell subjected to a central displacement X=60 mm. Owing to symmetry, only one quarter of the physical domain is modeled with 16×16 S4 elements, as presented in in Fig. 5. The present geometry can be found on works of Frikha *et al.* (2017), and Sze *et al.* (2004), among others, and is particularly popular due to the snapping behavior.

The geometrical properties of the shell are given by the length L=254, radius R=2540, the angle θ=0.1 rad and various thicknesses h. The elastoplastic FG material properties are listed in Tables 2 and 3. The non-linear mechanical responses of FG metal-ceramic panels shallow hinged cylindrical roof are given in Fig. 6 for different material composition exponents p.

On the other hand, elastic and elastoplastic deformed shapes of hinged FGM cylindrical roof subjected to a concentrated load for power law index p=10, are given in Fig. 7. Observing these figures, it is easily deduced that elastoplastic central deflections are larger than elastic ones and the greater deflection is provided by metal and small

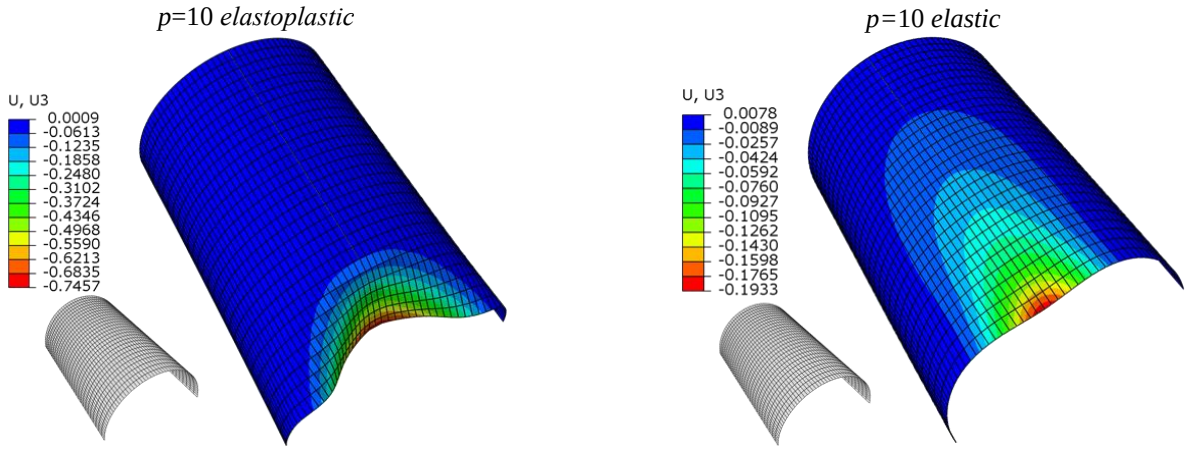

(a) (b)

Fig. 11 Elastoplastic and elastic deformed shapes of the semi cylindrical configuration for power law index p=10, U3: radial displacement of the semi-cylindrical

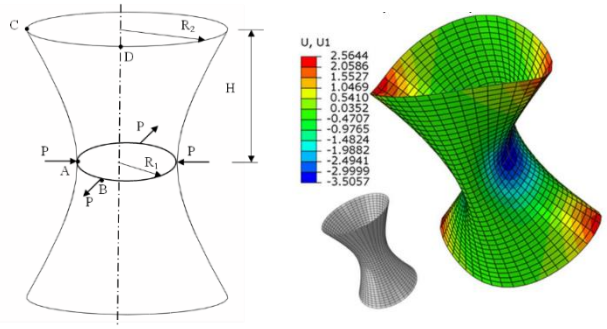

(a) (b)

Fig. 11 Hyperboloidal FGM shell subjected to alternating radial forces: (a) Geometrical properties, (b) Elastoplastic deformed shape p=10

Table 4 Radial deflection at point A ($-W_A$) of the elastoplastic Hyperboloidal FGM shell

F/F_{max} ceramic	p=0.2		p=5		p=10		Metal	
	elastoplastic	elastic	elastoplastic	elastic	elastoplastic	elastic	elastoplastic	elastic
0	0	0	0	0	0	0	0	0
0.2	0.258	0.370	0.369	0.741	0.715	0.817	0.780	1.030	1.016
0.4	0.511	0.833	0.720	1.614	1.303	1.728	1.403	2.021	1.735
0.7	0.864	2.043	1.179	2.699	1.938	2.784	2.057	3.039	2.442
0.9	1.077	2.656	1.437	3.208	2.257	3.286	2.384	3.556	2.786
1	1.176	2.897	1.554	3.429	2.396	3.505	2.526	3.781	2.935

deflection is given by ceramic due to its large mechanical proprieties making the FGM shell stiffer.

Fig. 8 exhibits the effect of the slenderness ratio h/R on the central deflection of the hinged FGM cylindrical roof subjected to a concentrated load for the selected values of power law index (p=2; 10) and for metal. It is found that central deflection of the FGM shell decreases as the slenderness ratio rises considering the same applied load and material composition p.

4.2.2 Semi-cylindrical FG Shell loaded with an end pinching force

The second example considers a semi-cylindrical shell subjected to an end pinching force at the middle of the free-hanging circumferential periphery. The other circumferential periphery is fully clamped. Along its longitudinal edges, the vertical deflection and the rotation about the Y-axis are restrained. The cylinder length is L = 3.048 and the radius R=1.016 with thickness h=0.03. Owing to symmetry, one-quarter of the shell is modeled and a commonly employed mesh for four-node shell elements is 28×28, as shown in Fig. 9.

The elastoplastic FG material properties are described in Tables 2 and 3. The present geometry has been considered in many references investigating geometric non-linearity of shells Sze *et al.* (2004) and Fontes *et al.* (2003), among others.

The maximum applied load at the middle of the free edge is fixed to F=1×10^6. Elastic and elastoplastic behaviors at point A of the FG metal-ceramic semi-cylindrical shell subjected to a pinching force are plotted in Fig. 10 for different power-law index. Fig. 11 represents elastoplastic and elastic deformed shapes of the semi cylindrical configuration for power law index p=10.

As may be seen, elastoplastic displacements are more important than elastic ones considering the same applied load and the same power law index. It can be also noticeable, from Fig. 11, that power law exponent p has important influence on both elastic and elastoplastic behaviors of the FG metal-ceramic semi-cylindrical shell subjected to a pinching force.

4.2.3 Hyperboloidal FGM shell subjected to alternating radial forces

The third example considers a hyperboloidal FGM under two inward and two outward point loads to evaluate the performance of the present approach in the case of large rotations. Many researchers, dealing with nonlinear geometrically problem, have considered this geometry, namely, Arciniega and Reddy (2007) and Mars *et al.* (2017). Due to symmetry, one-eighth of the structure is modeled

Table 5 Radial deflection at point B (W_B) of the elastoplastic Hyperboloidal FGM shell

F/F_{max}	ceramic	p=0.2		p=5		p=10		Metal	
		elastoplastic	elastic	elastoplastic	elastic	elastoplastic	elastic	elastoplastic	elastic
0	0	0	0	0	0	0	0	0	0
0.1	0.128	0.184	0.184	0.362	0.361	0.397	0.396	0.525	0.525
0.3	0.380	0.563	0.536	1.121	0.984	1.216	1.061	1.473	1.321
0.6	0.501	0.820	0.699	1.544	1.228	1.642	1.314	1.895	1.590
0.8	0.728	1.584	0.991	2.191	1.604	2.256	1.694	2.432	1.973
1	0.934	2.191	1.237	2.577	1.876	2.624	1.966	2.771	2.237

with 10×20 S4 elements, as illustrated in Fig. 12. The geometrical properties of the shell are given by the radius R_1=7.5, R_2=15, the half-height H=20 and the thickness h=0.04. The maximum applied load $P=2\times10^5$. The elastoplastic FG material properties are described in Tables 2 and 3. The radius of the hyperboloidal shell can be expressed using the following equation

$$R(z):\ R_1\sqrt{1+\left(\frac{z\sqrt{3}}{20}\right)^2} \tag{36}$$

Elastic and elastoplastic behaviors at point A and B of the FG metal-ceramic hyperboloidal shell subjected to radial forces are examined for several material composition exponents p. Tables 4 and 5, list elastic and elastoplastic radial deflections at point A and B for different values of power law index p.

It should pointed out that there are large differences between elastoplastic and elastic deflection values. For the same load and the same volume fraction value, elastoplastic deflections are larger than elastic ones.

The power index has a significant effect on the both elastic and elastoplastic behaviors of the hemispherical shell subjected to uniform load. In order to emphasize the effect of power low index on the elastoplastic response of the FGM hyperboloidal shell, Tables 6 and 7 tabulate elastoplastic radial deflections at point C and D for various values of power law index p.

It should be pointed out that the increase in the material power index leads to an increase in the deflection of the FGM Hyperboloidal structure. This is because that as increasing the value of material power index the percentage of metal phase will rise. By reason of aluminum has lower elastic material proprieties, thus makes such FGM shells more flexible.

Those tests demonstrate the robustness of the present FEM using ABAQUS/UMAT and its applicability to arbitrary shell geometries and coupled material and geometric non-linearities.

5. Conclusions

In this research, a numerical approach to analyze the geometrical non-linear static response of elastoplastic

Table 6 Elastoplastic Radial deflection at point C (W_C) of the elastoplastic Hyperboloidal FGM shell

F/F_{max}	ceramic	p=0.2	p=2	p=5	p=10	metal
0	0	0	0	0	0	0
0.2	0.246	0.350	0.753	0.607	0.686	0.941
0.4	0.481	0.762	1.494	1.278	1.405	1.713
0.6	0.698	1.416	2.026	1.872	1.966	2.180
0.7	0.798	1.723	2.207	2.078	2.158	2.344
0.9	0.981	2.144	2.469	2.375	2.434	2.579
1	1.06	2.289	2.564	2.483	2.535	2.661

Table 7 Elastoplastic Radial deflection at point D ($-W_D$) of the elastoplastic Hyperboloidal FGM shell

F/F_{max}	ceramic	p=0.2	p=2	p=5	p=10	metal
0	0	0	0	0	0	0
0.1	0.125	0.178	0.388	0.312	0.353	0.516
0.3	0.372	0.550	1.205	0.981	1.108	1.469
0.6	0.719	1.575	2.262	2.094	2.198	2.435
0.8	0.926	2.202	2.609	2.494	2.567	2.736
1	1.110	2.548	2.830	2.739	2.798	2.931

FGM-shell structures is presented. The material properties are introduced according to the integration points via the implementation of the user-material UMAT subroutine into ABAQUS software. To the best knowledge of the authors, there are no further accessible documents in literature on ABAQUS implementation of elastoplastic and geometrical non-linear response of the ceramic particle-reinforced metal-matrix FGM plate/shell structures. The Mori-Tanaka model is used for locally predicting the effective elastic FGM properties and self-consistent method of Suquet for the homogenization of the elastoplastic Ludwik hardening law, which preserves the reduced computational time of the model. The main contribution of the present research is to form a convenient basis, for subsequent comparison, to analyze the elastoplastic geometrically nonlinear FG structures. The accuracy of the developed nonlinear solution procedures is well assessed through three non-trivial benchmark problems taken from the literature are examined. The influence of the material composition is investigated. The power index has a significant effect on the both elastic and elastoplastic behaviors, an increase in the material power index leads to an increase in the deflection of the FGM structure.

Acknowledgements

The work is carried out thanks to the support and funding allocated to the Unit of Mechanical and Materials Production Engineering (UGPMM/UR17ES43) by the Tunisian Ministry of Higher Education and Scientific Research.

References

Abdelaziz, H.H., Meziane, M.A.A., Bousahla, A.A., Tounsi, A., Mahmoud, S.R. and Alwabli, A.S. (2017), "An efficient hyperbolic shear deformation theory for bending, buckling and free vibration of FGM sandwich plates with various boundary conditions", *Steel Compos. Struct.*, **25**(6), 693-704.

Arciniega, R.A. and Reddy, J.N. (2007), "Tensor-based finite element formulation for geometrically nonlinear analysis of shell structures", *Comput. Meth. Appl. Mech. Eng.*, **196**(4-6), 1048-1073.

Attia, A., Bousahla, A.A., Tounsi, A., Mahmoud, S.R. and Alwabli, A.S. (2018), "A refined four variable plate theory for thermoelastic analysis of FGM plates resting on variable elastic foundations", *Struct. Eng. Mech.*, **65**(4), 453-464.

Autay, R., Koubaa, S., Wali, M. and Dammak, F. (2017), "Numerical implementation of coupled anisotropic plasticity-ductile damage in sheet metal forming process", *J. Mech.*, **34**(4), 417-430.

Baltacıoglu, A.K., Civalek, O., Akgoz, B. and Demir, F. (2011), "Large deflection analysis of laminated composite plates resting on nonlinear elastic foundations by the method of discrete singular convolution", *Int. J. Press. Vess. Pip.*, **88**(8-9), 290-300.

Bao, G. and Wang, L. (1995), "Multiple cracking in functionally graded ceramic/metal coatings", *Int. J. Sol. Struct.*, **32**(19), 2853-2871.

Barati, M.R. and Shahverdi, H. (2016), "A four-variable plate theory for thermal vibration of embedded FG nanoplates under non-uniform temperature distributions with different boundary conditions", *Struct. Eng. Mech.*, **60**(4), 707-727.

Beldjelili, Y., Tounsi, A. and Mahmoud, S.R. (2016), "Hygro-thermo-mechanical bending of S-FGM plates resting on variable elastic foundations using a four-variable trigonometric plate theory", *Smart Struct. Syst.*, **18**(4), 755-786.

Belhassen, L., Koubaa, S., Wali, M. and Dammak, F. (2016), "Numerical prediction of springback and ductile damage in rubber-pad forming process of aluminum sheet metal", *Int. J. Mech. Sci.*, **117**, 218-226.

Belhassen, L., Koubaa, S., Wali, M. and Dammak, F. (2017), "Anisotropic effects in the compression beading of aluminum thin-walled tubes with rubber", *Thin-Wall. Struct.*, **119**, 902-910.

Bellifa, H., Bakora, A., Tounsi, A., Bousahla, A.A. and Mahmoud, S.R. (2017), "An efficient and simple four variable refined plate theory for buckling analysis of functionally graded plates", *Steel Compos. Struct.*, **25**(3), 257-270.

Bellifa, H., Benrahou, K.H., Hadji, L., Houari, M.S.A. and Tounsi, A. (2016), "Bending and free vibration analysis of functionally graded plates using a simple shear deformation theory and the concept the neutral surface position", *J. Braz. Soc. Mech. Sci. Eng.*, **38**(1), 265-275.

Ben Said, L., Mars, J., Wali, M. and Dammak, F. (2017), "Numerical prediction of the ductile damage in single point incremental forming process", *Int. J. Mech. Sci.*, **131**, 546-558.

Bennoun, M., Houari, M.S.A. and Tounsi, A. (2016), "A novel five variable refined plate theory for vibration analysis of functionally graded sandwich plates", *Mech. Adv. Mater. Struct.*, **23**(4), 423-431.

Bocciarelli, M., Bolzon, G. and Maier, G. (2008), "A constitutive model of metal-ceramic functionally graded material behavior), pp. formulation and parameter identification", *Comput. Mater. Sci.*, **43**(1), 16-26.

Bouderba, B., Houari, M.S.A., Tounsi, A. and Mahmoud, S.R. (2016), "Thermal stability of functionally graded sandwich plates using a simple shear deformation theory", *Struct. Eng. Mech.*, **58**(3), 397-422.

Bouhadra, A., Tounsi, A., Bousahla, A.A., Benyoucef, S. and Mahmoud, S.R. (2018), "Improved HSDT accounting for effect of thickness stretching in advanced composite plates", *Struct. Eng. Mech.*, **66**(1), 61-73.

Bourada, M., Kaci, A., Houari, M.S.A. and Tounsi, A. (2015), "A new simple shear and normal deformations theory for functionally graded beams", *Steel Compos. Struct.*, **18**(2), 409-423.

Bousahla, A.A., Houari, M.S.A., Tounsi, A. and Adda Bedia, E.A. (2014), "A novel higher order shear and normal deformation theory based on neutral surface position for bending analysis of advanced composite plates", *Int. J. Comput. Meth.*, **11**(6), 1350082.

Civalek, O. (2008), "Analysis of thick rectangular plates with symmetric cross-ply laminates based on first-order shear deformation theory", *J. Compos. Mater.*, **42**(26), 2853-2867.

Civalek, O. (2013), "Nonlinear dynamic response of laminated plates resting on nonlinear elastic foundations by the discrete singular convolution-differential quadrature coupled approaches", *Compos.*: *Part B*, **50**, 171-179.

Demir, C., Mercan, K. and Civalek, O. (2016), "Determination of critical buckling loads of isotropic, FGM and laminated truncated conical panel", *Compos. Part B*, **94**, 1-10.

El-Haina, F., Bakora, A., Bousahla, A.A., Tounsi, A. and Mahmoud, S.R. (2017), "A simple analytical approach for thermal buckling of thick functionally graded sandwich plates", *Struct. Eng. Mech.*, **63**(5), 585-595.

Elmossouess, B., Kebdani, S., Bouiadjra, M.B. and Tounsi, A. (2017), "A novel and simple HSDT for thermal buckling response of functionally graded sandwich plates", *Struct. Eng. Mech.*, **62**(4), 401-415.

Fontes Valente, R.A., Natal Jorge, R.M., Cardoso, R.P.R., César de Sá, J.M.A. and Grácio, J.J.A. (2003), "On the use of an enhanced transverse shear strain shell element for problems involving large rotations", *Comput. Mech.*, **30**(4), 286-296.

Frikha, A. and Dammak, F. (2017), "Geometrically non-linear static analysis of functionally graded material shells with a discrete double directors shell element", *Comput. Meth. Appl. Mech. Eng.*, **315**, 1-24.

Frikha, A., Zghal, S. and Dammak, F. (2018), "Dynamic analysis of functionally graded carbon nanotubes-reinforced plate and shell structures using a double directors finite shell element", *Aerosp. Sci. Technol.*, **78**, 438-451.

Frikha, A., Hajlaoui, A., Wali, M. and Dammak, F. (2016), "A new higher order C0 mixed beam element for FGM beams analysis", *Compos. Part B*, **106**, 181-189.

Ghannad, M., Nejad, M.Z., Rahimi, G.H. and Sabouri, H. (2012), "Elastic analysis of pressurized thick truncated conical shells made of functionally graded materials", *Struct. Eng. Mech.*, **43**(1), 105-126.

GhannadPour, S.A.M. and Alinia, M.M. (2006), "Large deflection behavior of functionally graded plates under pressure loads", *Compos. Struct.*, **75**, 67-71.

Gunes, R., Aydin, M., Apalak, M.K. and Reddy, J.N. (2014), "Experimental and numerical investigations of low velocity impact on functionally graded circular plates", *Compos. Part B*: *Eng.*, **59**, 21-32.

Gürses, M., Civalek, O., Korkmaz, A. and Ersoy, H. (2009), "Free vibration analysis of symmetric laminated skew plates by discrete singular convolution technique based on first-order shear deformation theory", *Int. J. Numer. Meth. Eng.*, **79**(3), 290-313.

Hajlaoui, A., Triki, E., Frikha, A., Wali M. and Dammak, F. (2017), "Nonlinear dynamics analysis of FGM shell structures with a higher order shear strain enhanced solid-shell element", *Lat. Am. J. Sol. Struct.*, **14**(1), 72-91.

Hajlaoui, A., Jarraya, A., El Bikri, K. and Dammak, F. (2015),

"Buckling analysis of functionally graded materials structures with enhanced solid-shell elements and transverse shear correction", *Compos. Struct.*, **132**, 87-97.

Hebali, H., Tounsi, A., Houari, M.S.A., Bessaim, A. and Bedia, E.A.A. (2014), "A new quasi-3D hyperbolic shear deformation theory for the static and free vibration analysis of functionally graded plates", *J. Eng. Mech.*, **140**(2), 374-383.

Hosseini Tehrani, P. and Talebi, M. (2012), "Stress and temperature distribution study in a functionally graded brake disk", *Int. J. Automot. Eng.*, **2**(3), 172-179.

Jin, G., Te, Y., Me, X., Chen, Y., Su, X. and Xie, X. (2013), "A unified approach for the vibration analysis of moderately thick composite laminated cylindrical shells with arbitrary boundary conditions", *Int. J. Mech. Sci.*, **75**, 357-376.

Kar, V.R. and Panda, S.K. (2015), "Large deformation bending analysis of functionally graded spherical shell using FEM", *Struct. Eng. Mech.*, **53**(4), 661-679.

Lee, M., Park, I. and Lee, U. (2017), "An approximate spectral element model for the dynamic analysis of an FGM bar in axial vibration", *Struct. Eng. Mech.*, **61**(4), 551-561.

Liew, K.M., He, X.Q., Tan, M.J. and Lim, H.K. (2004), "Dynamic analysis of laminated composite plates with piezoelectric sensor/actuator patches using the FSDT mesh-free method", *Int. J. Mech. Sci.*, **46**(3), 411-431.

Mahi, A. and Tounsi, A. (2015), "A new hyperbolic shear deformation theory for bending and free vibration analysis of isotropic, functionally graded, sandwich and laminated composite plates", *Appl. Math. Model.*, **39**(9), 2489-2508.

Mars, J., Koubaa, S., Wali, M. and Dammak, F. (2017), "Numerical analysis of geometrically non-linear behavior of functionally graded shells", *Lat. Am. J. Sol. Struct.*, **14**(11), 1952-1978.

Mars, J., Wali, M., Jarraya, A., Dammak, F. and Dhiab. (2015), "A Finite element implementation of an orthotropic plasticity model for sheet metal in low velocity impact simulations", *Thin-Wall. Struct.*, **89**, 93-100.

Menasria, A., Bouhadra, A., Tounsi, A., Bousahla, A.A. and Mahmoud, S.R. (2017), "A new and simple HSDT for thermal stability analysis of FG sandwich plates", *Steel Compos. Struct.*, **25**(2), 157-175.

Mindiin, R.D. (1951), "Influence of rotary inertia and shear on flexural motion of isotropic elastic plates", *J. Appl. Mech.*, **18**, 31-38.

Moita, J.S., Araújo, A.L., Mota Soares, C.M., Mota Soares, C.A. and Herskovits, J. (2016), "Material and geometric nonlinear analysis of functionally graded plate-shell type structures", *Appl. Compos. Mater.*, **23**(4), 537-554.

Orlik, J. (2010), "Asymptotic homogenization algorithm for reinforced metal-matrix elastoplastic composites", *Compos. Struct.*, **92**(7), 1581-1590.

Pettermann, H.E., Huber, C.O., Luxner, M.H., Nogales, S. and Böhm, H.J. (2010), "An incremental Mori-Tanaka homogenization scheme for finite strain thermoelastoplasticity of mmcs", *Mater.*, **3**(1), 434-451.

Phung-Van, P., Nguyen-Thoi, T., Luong-Van, H. and Lieu-Xuan, Q. (2014), "Geometrically nonlinear analysis of functionally graded plates using a cell-based smoothed three-node plate element (CS-MIN3) based on the C0-HSDT", *Comput. Meth. Appl. Mech. Eng.*, **270**, 15-36.

Rahman, S. and Chakraborty, A. (2007), "A stochastic micromechanical model for elastic properties of functionally graded materials", *Mech. Mater.*, **39**(6), 548-563.

Reddy, J.N. (1984), "A refined nonlinear theory of plates with transverse shear deformation", *Int. J. Sol. Struct.*, **20**(9-10), 881-896.

Shankara, C.A. and Iyengar, N.G.R. (1996), "A C0element for the free vibration analysis of laminated composite plates", *J. Sound Vibr.*, **191**(5), 721-738.

Shaterzadeh, A. and Foroutan, K. (2016), "Post-buckling of cylindrical shells with spiral stiffeners under elastic foundation", *Struct. Eng. Mech.*, **60**(4), 615-631.

Suquet, P. (1997), "Effective properties of nonlinear composites", *Contin. Micromech.*, **377**, 197-264.

Sze, K.Y., Liua, X.H. and Lob, S.H. (2004), "Popular benchmark problems for geometric nonlinear analysis of shells", *Fin. Elem. Analy. Des.*, **40**(11), 1551-1569.

Talebitooti, M. (2013), "Three-dimensional free vibration analysis of rotating laminated conical shells: Layerwise differential quadrature (LW-DQ) method", *Arch. Appl. Mech.*, **83**(5), 765-781.

Tamura, I., Tomota, Y. and Ozawa, H. (1973), "Strength and ductility of Fe-Ni-C alloys composed of austenite and martensite with various strength", *Proceedings of the 3rd International Conference on Strength of Metals and Alloys, Cambridge: Institute of Metals*.

Tjong, S.C. and Ma, Z.Y. (2000), "Microstructural and mechanical characteristics of in situ metal matrix composites", *Mater. Sci. Eng.*, **29**(3-4), 49-113.

Trabelsi, S., Frikha, A., Zghal, S. and Dammak, F. (2018), "Thermal post-buckling analysis of functionally graded material structures using a modified FSDT", *Int. J. Mech. Sci.*, **144**, 74-89.

Tu, T.M., Quoc, T.H. and Van Long, N. (2017), "Bending analysis of functionally graded plates using new eight-unknown higher order shear deformation theory", *Struct. Eng. Mech.*, **62**(3), 311-324.

Vaghefi, R., Hematiyan, M.R. and Nayebi, A. (2016), "Three-dimensional thermo-elastoplastic analysis of thick functionally graded plates using the meshless local Petrov-Galerkin method",*Eng. Analy. Bound. Elem.*, **71**, 34-49.

Wali, M., Autay, R., Mars, J. and Dammak, F. (2016), "A simple integration algorithm for a non-associated anisotropic plasticity model for sheet metal forming", *Int. J. Numer. Meth. Eng.*, **107**(3), 183-204.

Wali, M., Chouchene, H., Ben Said, L. and Dammak, F. (2015), "One-equation integration algorithm of a generalized quadratic yield functions with Chaboche non-linear isotropic/kinematic hardening", *Int. J. Mech. Sci.*, **92**, 223-232.

Williamson, R.L., Rabin, B.H. and Drake, J.T. (1993), "Finite element analysis of thermal residual stresses at graded ceramic/metal interfaces), part I), pp. model description and geometrical effects", *J. Appl. Phys.*, **74**(2), 1310-1320.

Woo, J. and Merguid, S.A. (2001), "Non-linear analysis of functionally graded plates and shallow shells", *Int. J. Sol. Struct.*, **38**(42-43), 7409-7421.

Xu, G., Huang, H. and Han, Q. (2018), "Study on postbuckling of axial compressed elastoplastic functionally graded cylindrical shells", *Mech. Adv. Mater. Struct.*, **25**(10), 820-828.

Yang, J. and Shena, H.S. (2003), "Non-linear analysis of functionally graded plates under transverse and in-plane loads", *Int. J. Non-Lin. Mech.*, **38**(4), 467-482.

Younsi, A., Tounsi, A., Zaoui, F.Z., Bousahla, A.A. and Mahmoud, S.R. (2018), "Novel quasi-3D and 2D shear deformation theories for bending and free vibration analysis of FGM plates", *Geomech. Eng.*, **14**(6), 519-532.

Yu, J. and Kidane, A. (2014), "Modeling functionally graded materials containing multiple heterogeneities", *Acta Mech.*, **225**(7), 1931-1943.

Zghal, S., Frikha, A. and Dammak, F. (2018a), "Free vibration analysis of carbon nanotube-reinforced functionally graded composite shell structures", *Appl. Math. Modell.*, **53**, 132-155.

Zghal, S., Frikha, A. and Dammak, F. (2017), "Static analysis of

functionally graded carbon nanotube-reinforced plate and shell structures", *Compos*. *Struct*., **176**, 1107-1123 .

Zghal, S., Frikha, A. and Dammak, F. (2018b), "Mechanical buckling analysis of functionally graded power-based and carbon nanotubes-reinforced composite plates and curved panels", *Compos*. *Part B*, **150**(1), 165-183.

Zghal, S., Frikha, A. and Dammak, F. (2018c), "Non-linear bending analysis of nanocomposites reinforced by graphene-nanotubes with finite shell element and membrane enhancement", *Eng*. *Struct*., **158**, 95-109.

Zhao, X. and Liew, KM. (2009), "Geometrically nonlinear analysis of functionally graded shells", *Int*. *J*. *Mech*. *Sci*., **51**, 131-144.

Zidi, M., Tounsi, A., Houari, M.S.A. and Bég, O.A. (2014), "Bending analysis of FGM plates under hygro-thermo-mechanical loading using a four variable refined plate theory", *Aerosp*. *Sci*. *Technol*., **34**, 24-34.

PL